A Wearable Prototype Measuring PtcCO₂ and SpO₂

Kleo Golemi^{†*}, Evan Apinis^{†*}, Isil Isiksalan[†], Vladimir Vakhter[†], and Ulkuhan Guler[†]

Department of Electrical and Computer Engineering, Worcester Polytechnic Institute, Worcester, MA 01609 USA

Abstract—The proper functioning of the respiratory system is evaluated by monitoring the exchange of blood oxygen and carbon dioxide. While wearable devices for monitoring both blood oxygen and carbon dioxide are emerging, wearable carbon dioxide monitors remain relatively rare. This paper introduces a novel wearable prototype that integrates the measurement of transcutaneous carbon dioxide and peripheral blood oxygen saturation on a miniaturized custom-designed printed circuit board. The device employs a fluorescent sensing film consisting of two distinct luminophore types and utilizes the time-domain dual lifetime referencing technique to enhance measurement accuracy by mitigating the effects of confounding factors. Thorough testing on human subjects validated the prototype's functionality, comparing its performance against commercial clinical devices. The prototype effectively tracked changes in transcutaneous carbon dioxide induced by hyperventilation, with a resolution as low as 1 mmHg. Additionally, blood oxygen saturation measurements were tested on human subjects to compare our prototypes' performance to that of clinical devices. The results confirm the potential of the proposed novel wearable for prolonged use with minimal maintenance and underscore its significance in advancing wearable health monitoring technologies.

Index Terms—Transcutaneous carbon dioxide sensing, PtcCO₂, noninvasive blood gas monitoring, physiological monitoring, fluorescence sensing, t-DLR, pulse oximeter, SpO₂.

I. INTRODUCTION

The efficient exchange of gases, particularly oxygen (O_2) and carbon dioxide (CO_2) , within the respiratory system is a key indicator of a healthy physiological balance [1], [2]. In scenarios where impaired gas exchange results in CO_2 accumulation due to slow and shallow breathing, respiratory depression can occur. This condition contributed to ~ 4.5 million deaths in the U.S. between 1999 and 2018 [3]. Similarly, impaired gas exchange leading to an O_2 deficiency can result in hypoxemia, a condition that severely compromises organ function and can cause critical health issues if not detected early [4], [5]. Monitoring the real-time dynamics of vital blood gases can facilitate early detection of disruptions and provide valuable insights into various physiological conditions [6], [7].

Traditionally, blood gases are measured in a clinical setting using arterial blood gas (ABG) analysis. This invasive procedure involves arterial punctures, regularly performed in hospitals to diagnose and evaluate acutely ill patients [8], [9]. Although generally considered safe, ABG analysis can be uncomfortable and poses a small risk of complications, such

This material is based upon work supported in part by the National Science Foundation (NSF) under Grant ECCS-2143898 and National Institute of Health (NIH) under Grant 1R01HL172293-01. Corresponding author: Ulkuhan Guler: uguler@wpi.edu.

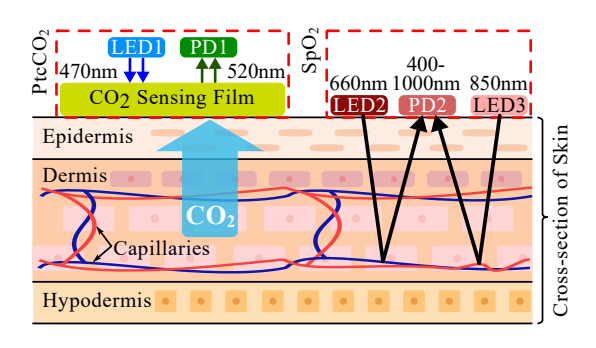


Fig. 1. Operational principles of fluorescent ${\rm PtcCO_2}$ and reflective ${\rm SpO_2}.$

as pain, hematoma, or more serious issues like nerve damage or thrombosis, due to the invasive nature of the sampling [10].

Noninvasive surrogate methods, such as transcutaneous carbon dioxide ($PtcCO_2$) monitoring [11], provide an alternative by allowing real-time assessment of CO_2 diffusion from the skin, directly correlating with the arterial partial pressure of CO_2 ($PaCO_2$) [12], [13]. Furthermore, peripheral blood oxygen saturation (SpO_2), typically measured using pulse oximetry, offers a prevalent noninvasive assessment of oxygenation [14], [15]. SpO_2 serves as a noninvasive surrogate for arterial oxygen saturation (SaO_2), indicating the percentage of oxygenated hemoglobin (oxy-hemoglobin, HbO_2) relative to the concentration of effective hemoglobin, which includes both deoxygenated hemoglobin (deoxy-hemoglobin, RHb) and oxygenated hemoglobin, in arterial blood [16].

To our knowledge, this paper introduces the first preliminary noninvasive wearable prototype, integrating methodologies for estimating $PtcCO_2$ through fluorescence sensing and SpO_2 via pulse oximetry to assess respiratory health, as depicted in Fig. 1. The subsequent sections of this manuscript are organized as follows. Section II details the sensing mechanisms behind the measured modalities. Section III explains the system implementation, covering hardware, firmware, and post-processing algorithms. Section IV presents the results of human subject tests, including $PtcCO_2$ and SpO_2 measurements with the proposed wearable and commercial gold standards and offers a discussion on benchmarking, followed by the concluding remarks in Section V.

II. SENSING METHODOLOGY

A. PtcCO₂ Sensing Method

The $PtcCO_2$ sensing method utilizes a specialized fluorescent sensing film (SP-CD1-D5-rMy-US by Pre-Sens Precision Sensing) that is integral to our design. The film contains two types of luminophores: one sensitive to CO_2 fluctuations, termed the sensitive luminophore, and another unaffected

^{*} These authors contributed equally.

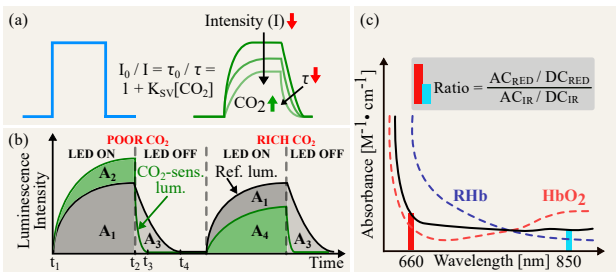


Fig. 2. Sensing methods: (a) relationship between CO₂ amount and fluorescence intensity and lifetime; (b) illustration of the time-domain dual lifetime referencing technique (adapted from [20]); and (c) relationship between AC and DC components in SpO₂ measurements.

by such changes, known as the reference luminophore [17]. The dual luminophore setup is excited at a wavelength of 470 nm (blue), resulting in the emission of green light at a wavelength of 520 nm, illustrated in Fig. 2a. To address the challenges posed by confounding factors in intensity-based luminescence measurements, elaborated in [18], we utilize the dual lifetime referencing (DLR) technique [19]. The DLR process is conducted in the time domain, designated as t-DLR, which integrates signal segments during the LED's ON and OFF periods, as depicted in Fig. 2b. The A_{ON} region represents the luminescence intensity during the LED ON phase according to

$$\frac{A_{\rm ON}}{C_{\rm EXT}} = \frac{L_{\rm SEN_0}}{PCO_2} \cdot \int_t L_{\rm SEN\text{-}ON}(t) dt + L_{\rm REF_0} \cdot \int_t L_{\rm REF\text{-}ON}(t) dt, (1)$$

where $C_{\rm EXT}$ contains the confounding factors, $L_{\rm SEN_0}$ and $L_{\rm REF_0}$ are luminescence constants, PCO_2 is the amount of CO_2 , $L_{\rm SEN-ON}(t)$ and $L_{\rm REF-ON}(t)$ are the luminescence intensity of the respective sensitive and reference luminophore.

In conditions of low CO_2 , the luminescence intensity from the sensitive luminophore is more pronounced, resulting in A_{ON} being visually represented by the sum of A_2 and A_1 . In conditions of high CO_2 , the luminescence intensity from the sensitive luminophore is reduced to A_4 , and A_{ON} is thus represented by the sum of A_4 and A_1 . The A_{OFF} region captures the decay of luminescence following the LED's deactivation, primarily reflecting the activity of the reference luminophore, and is defined by

$$A_{\text{OFF}} = C_{\text{EXT}} \cdot L_{\text{REF}_0} \left(\int_t L_{\text{REF-OFF}}(t) \right),$$
 (2)

where L_{REF_0} is a luminescence constant, and $L_{REF-OFF}(t)$ is the luminescence intensity of the reference luminophore. This decay characteristic is crucial for effective t-DLR, especially in distinguishing between various CO_2 concentrations.

B. SpO₂ Sensing Method

The SpO_2 percentage is measured using pulse oximetry, a noninvasive technique that utilizes red and infrared (IR) light-emitting diodes (LEDs). In this reflective approach, LEDs sequentially pulse light onto the skin, where they further interact with HbO_2 and RHb in the blood. The varying absorption of these wavelengths by hemoglobin allows for the differentiation between oxygenated and deoxygenated states. The light that is not absorbed by the blood is reflected and detected by

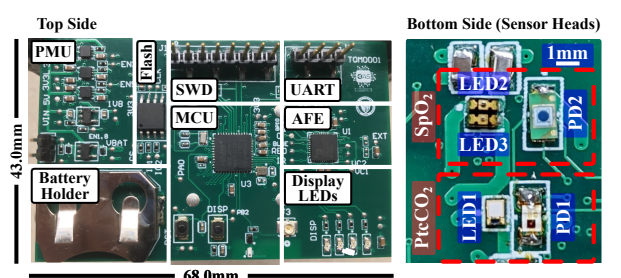


Fig. 3. Sensing board for PtcCO₂ and SpO₂. Adapted from [22].

a photodiode (PD) as depicted in Fig. 1. By measuring the intensity of this reflected light at each wavelength, we can calculate the ratio of red to IR absorption, which is used to determine the ${\rm SpO}_2$ percentage. The calculation is based on

$$R = \left[\frac{AC_{RED}}{DC_{RED}}\right] / \left[\frac{AC_{IR}}{DC_{IR}}\right],\tag{3}$$

where R is the SpO_2 ratio, $\mathrm{AC}_{\mathrm{RED}}$, $\mathrm{AC}_{\mathrm{IR}}$, $\mathrm{DC}_{\mathrm{RED}}$, and $\mathrm{DC}_{\mathrm{IR}}$ are recorded red and IR signals representing the pulsatile ("alternating current") and non-pulsatile ("direct current") compartments of the blood vessel, accordingly [21] (Fig. 2c).

III. SYSTEM IMPLEMENTATION

A. Hardware Implementation

The proposed wearable dual-mode monitor builds on our previous transcutaneous oxygen (PtcO₂) prototype [22]. The PtcCO₂ modality required the green-sensitive version of PD1 (SD019-141-411-G by Advanced Photonix) to capture the light emitted from the fluorescent sensing film, while LED1 (LXZ1-PR0 by Lumileds) is used for excitation. The SpO₂ sensor head incorporates combined LED2 and LED3 (VSMD66694 by Vishay) along with PD2 (S13773 by Hamamatsu), as shown in Figs. 1 and 3. The remaining electronic modules, including detailed performance characterizations such as the noise and bandwidth of the TIA and system power estimates, are described in [22], [23].

B. Firmware Implementation

The main operation of the firmware is thoroughly described in [23]. To avoid redundancy, the following subsections will highlight the newly implemented features only.

1) Timer Configuration: The onboard t-DLR technique and the pulse oximeter share the same microcontroller unit (MCU), facilitating a concurrent sensing process that enhances monitoring efficiency. This process is managed by the internal timer TIM17, set to trigger at 36 Hz for real-time data acquisition, as depicted in Fig. 4. Upon a TIM17 interrupt, the MCU initiates data capture from the AFE. The data, temporarily stored in the AFE's FIFO buffer, undergoes initial pre-processing steps such as filtering and downsampling. If the waveform buffer is not full, the processed data is saved; otherwise, TIM17 is disabled to prevent data loss during SpO₂ post-processing. Following SpO₂ analysis, the device is reconfigured for PtcCO₂ measurement, including adjustments to the optical path and register settings. After completing PtcCO₂ data acquisition and applying t-DLR algorithms, the TIM17 interrupt is reactivated to resume normal operation.

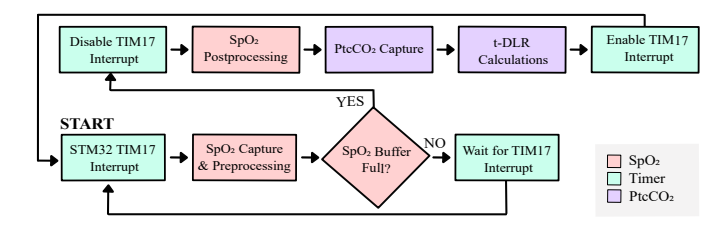


Fig. 4. STM32 data collection processing flow.

C. Algorithm Implementation

Wearable device applications, especially those for monitoring vital signs, require real-time onboard computations with minimal power consumption [24]. To meet these demands, we employed a regression algorithm to compute the A_{OFF} region, given in Eq. 2, crucial for the t-DLR technique.

1) Fluorescence Lifetime Calculation: The sensing film's fluorescence exhibits an exponential decay, characterized by the lifetime value τ . Lifetime calculation requires an accurate estimation of the exponential change rate, DC offset, and scaling factor for precise signal interpretation. These parameters are obtained using a closed-form analytical regression technique [25], which reconstructs an exponential curve through a set of linear operations.

regression algorithm, employed to calculate required τ in the t-DLR technique, the identifies optimal parameters to fit a curve of the form "Output = Scaling Factor $\times e^{-\tau \times t}$ + DC Offset", where t is time. However, predefined Scaling Factor and DC Offset values in this context may introduce inaccuracies. To mitigate this, we adjust the waveform input by appending additional tail values, thereby fixing the DC Offset and partially constraining the Scaling Factor. This modification reduces the degrees of freedom to one, namely τ , enhancing the precision of our exponential change rate calculations for this particular application. Despite the mathematical complexity of these operations, they are deterministic and efficient, yielding the fit parameters in just 0.004 seconds.

2) Processing Algorithms: Expanding on the setup for SpO₂ measurement [26], various signal pre-processing techniques were applied to improve the quality of photoplethysmogram (PPG) waveforms and enhance the signal-to-noise ratio (SNR). Configuring the AFE for 8 repeated pulses with a 2 μ s pulse width resulted in a 9 dB SNR increase compared to a single pulse configuration. The relationship between the number of pulses, p, and SNR in dB is given by $3 \cdot \log_2(p)$ [27]. The pulse oximeter operated at a sampling rate of 36 Hz. To counteract ambient noise and aliasing effects, downsampling and a 17th-order FIR lowpass filter with a passband at 5 Hz and a stopband at 10 Hz were employed, achieving 80 dB of attenuation and effectively isolating the PPG signal from aliased noise. To extract vital metrics from the PPG signals, we implemented post-processing via MCU functions, including Discrete Fourier Transform (DFT), converting the time-domain signals to the frequency domain, revealing frequencies corresponding to heart rate. These metrics are crucial for calculating the modal heart rate during data collection.

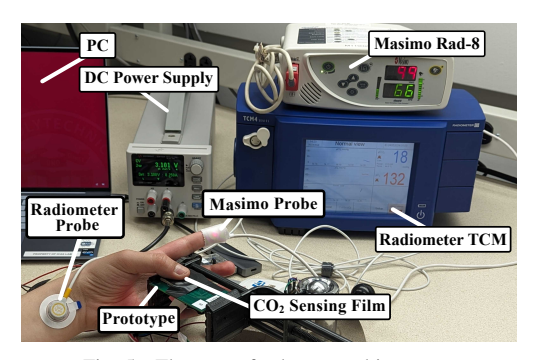


Fig. 5. The setup for human subject tests.

IV. MEASUREMENTS AND RESULTS

A. PtcCO₂ Testing

For $PtcCO_2$ measurements, we conducted sensor characterization and checked the t-DLR ratio under controlled conditions, similar to an experiment performed in [18]. In order to measure the resolution, we used a gas flow chamber and insulated vial. Temperature and humidity were fixed while PCO_2 was incrementally swept by 0.1% – the minimum CO_2 percentage measurable by our gas flow meter – at 7-minute intervals to ensure the sensor reached equilibrium. This process continued until a change in the output ratio was observed. The corresponding PCO_2 value was then converted to mmHg, revealing that the sensor could detect changes as small as 1 mmHg. This resolution is comparable to benchtop devices, shown in Table I, and marks a notable improvement over prior work [18].

To validate our findings and assess a practical application, a human subject test was performed with the prototype to gauge the resolution of the t-DLR algorithm and response to detecting PtcCO₂. To evaluate the performance, the prototype was placed on the thumb of the participant as depicted in Fig. 5. For the test, the participant was also attached to Radiometer TCM4 CombiM [30] with the tc Sensor 84 probe, with the capabilities of reading PtcCO₂ for comparison. After both devices reached stabilization, data capture began, as reflected by the x-axis in Fig. 6a starting at 40 minutes. The participant was then instructed to hyperventilate for 3.5 minutes to determine whether the device could detect changes in CO₂. Following this, we allowed time for the devices to recover. The results are presented in Fig. 6a, where the luminescence ratio is inversely proportional to PtcCO₂. Hence, we plotted the inverse of the luminescence ratio to better align the signals. Note that the commercial device's measurement values are displayed on the right y-axis.

B. SpO_2 Testing

To evaluate the performance of the pulse oximeter presented in this study, we compared it with the Masimo Rad-8 [28], a commercially available benchtop device that uses transmissive sensing. The Masimo device provides a continuous stream of ${\rm SpO}_2$ and heart rate data every second, offering a benchmark for comparison. In contrast, our pulse oximeter computes these measurements approximately every fifty seconds. To ensure consistency in this comparison, average results from

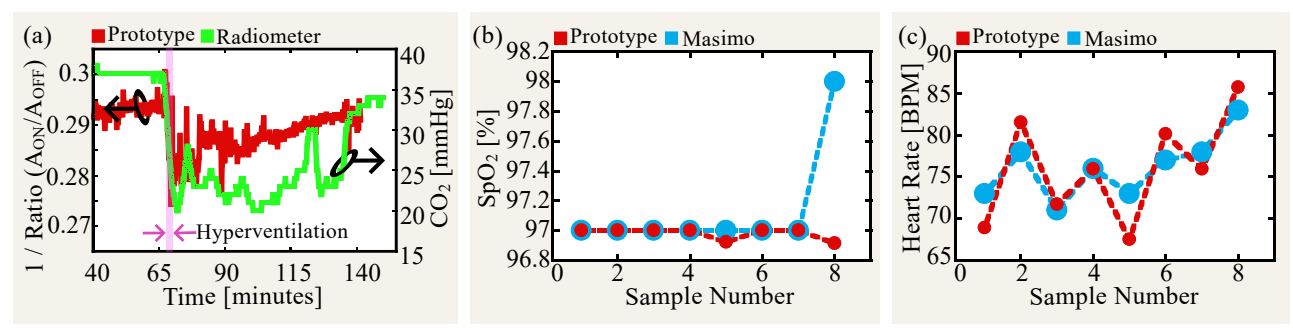


Fig. 6. (a) Fingertip PtcCO₂ test results for our prototype and Radiometer device; (b) mode values for SpO₂ measured with our prototype and Masimo device; and (c) mode values for heart rate measured with our prototype and Masimo devices.

TABLE I
COMPARISON OF PERFORMANCE PARAMETERS OF TRANSCUTANEOUS CARBON DIOXIDE AND OXYGEN SATURATION MONITORS

Parameter	[28]	[29]	[30]	[18]	This Work
	2009	2023	2018	2023	2024
Modalities SpO ₂ Range (%) SpO ₂ Resolution (%) HR Range HR Resolution (BPM) PtcCO ₂ Range (mmHg) PtcCO ₂ Resolution (mmHg)	SpO ₂ /HR	SpO ₂ /Ptc(C)O ₂ /HR	Ptc(C)O ₂	PtcCO ₂	SpO ₂ /PtcCO ₂ /HR
	1–100	1-100	N/A	N/A	N/A
	1	1	N/A	N/A	0.1
	25–240	30-250	N/A	N/A	60–240
	1	1	N/A	N/A	1.41
	N/A	0-200	O-200	0-76	0–76
	N/A	0.1	1	5	1
Form Factor Pulse Oximetry Technique PtcCO ₂ Sensing Technique	Bench Top	Bench Top	Bench Top	Wearable	Wearable
	Transmissive	Reflective	N/A	N/A	Reflective
	N/A	Electrochemical	Electrochemical	Fluorescence	Fluorescence
Supply Voltage (V) Max. Power Consumption Transimpedance Gain $(k\Omega)$	100–240 AC	100–240 AC	100–240 AC	5 DC	3.3 DC
	120VA	N/A	70VA	30.1mW	N/A
	N/A	N/A	N/A	250	12.5–200

Note: N/A - not addressed. HR - heart rate. Ptc(C)O₂ denotes both PtcCO₂ and PtcO₂.

the Masimo were recorded during the operation cycle of our device. The test maintained consistent sensing locations by using two fingertips on the same hand. The SpO_2 percentages reported by the Masimo device and our prototype are displayed in Fig. 6b. The results confirm close performance compared to the Masimo, including identical measurements for six of the eight captured data points. Additionally, one of the remaining two points was within $\sim 1\%$ error. The only concern arises with the final data point, where the Masimo Rad-8 reported an increase in SpO_2 , while our pulse oximeter indicated a decrease. The variation was minor, between 98% and 96.9%. Considering that the healthy SpO_2 range is 95% to 100% [31], these measurements are promising.

The heart rate measured in beats per minute (BPM) is shown in Fig. 6c, displaying the data of an eight-minute capture window for both devices. Over this window, it can be seen that the heart rate measurements recorded on the presented prototype followed the trend or change in heart rate that was measured by the Masimo Rad-8 [28] device. Another metric worth noting is that for every data point except for sample number five, our prototype was within 5% of the heart rate value measured by Masimo Rad-8 [28].

Table I compares key specifications between commercial clinical devices and the proposed technology. It is important to underscore that the proposed prototype represents a unique advancement in the realm of miniaturized wearable devices, as it successfully integrates two pivotal blood gas parameters, PtcCO₂ and SpO₂. Notably, unlike [29] and [30], the proposed

prototype avoids the use of heating mechanisms, a major advancement for wearable blood gas monitors, to augment blood flow and molecule diffusion through the skin, thereby enhancing accuracy. For PtcCO₂ monitoring, we compared our device with commercial clinical devices, Sentec, and Radiometer TCMs. Our device delivers results comparable to bench-top devices, measuring between 0 and 76 mmHg with a 1-mmHg resolution, an improvement over the previous 5 mmHg [18] while offering a smaller footprint. This enhancement is due to the inclusion of the ADPD4100 AFE and the implementation of the t-DLR technique directly on the MCU, rather than relying on off-board post-processing. For pulse oximetry, comparisons were made with the Masimo Rad-8 [28], which measured heart rate between 25 and 250 BPM with a 1 BPM resolution. Our device measured 60 to 240 BPM with a 1.41 BPM resolution due to the limited buffer sizes of the utilized MCU. For SpO_2 measurements, our prototype displayed a resolution of 0.1% compared to 1%.

V. CONCLUSION

This study demonstrates the feasibility and efficacy of a novel wearable prototype for noninvasive monitoring of PtcCO₂ and SpO₂. To the best of our knowledge, this is the first instance of a device achieving the on-board measurement of both PtcCO₂ and SpO₂ concurrently. The prototype successfully registered changes in PtcCO₂ caused by hyperventilation, achieving a resolution as fine as 1 mmHg. The results validate the prototype's potential for accurate and reliable measurement of blood gases in a noninvasive manner.

ACKNOWLEDGMENT

We extend our appreciation to Tuna Berk Tufan for his guidance and support during this research. Additionally, we would like to thank Burak Kahraman for his assistance and valuable suggestions.

REFERENCES

- [1] I. Costanzo *et al.*, "Respiratory monitoring: Current state of the art and future roads," *IEEE Reviews in Biomedical Engineering*, vol. 15, pp. 103–121, 2020.
- [2] L. Rhein, Measures of Carbon Dioxide. Cambridge University Press, 2018, ch. 5, pp. 38–44.
- [3] H. Hedegaard et al., "Drug overdose deaths in the united states, 1999– 2020," 2021.
- [4] R. N. Pittman, "Oxygen transport in normal and pathological situations: defects and compensations," in *Regulation of Tissue Oxygenation*. Morgan & Claypool Life Sciences, 2011, ch. 7.
- [5] M. Sarkar et al., "Mechanisms of hypoxemia," Lung india, vol. 34, no. 1, pp. 47–60, 2017.
- [6] U. Guler et al., "Emerging blood gas monitors: How they can help with COVID-19," IEEE Solid-State Circuits Magazine, vol. 12, no. 4, pp. 33–47, 2020.
- [7] C.-J. Lim et al., "Wearable, luminescent oxygen sensor for transcutaneous oxygen monitoring," ACS applied materials & interfaces, vol. 10, no. 48, pp. 41 026–41 034, 2018.
- [8] A. Goenka et al., "Neonatal blood gas sampling methods," South African Journal of Child Health, vol. 6, no. 1, pp. 3–9, 2012.
- [9] L. M. Rhein, Blood Gas and Pulmonary Function Monitoring. Wolters Kluwer Health, 2016, ch. 30.
- [10] S. C. Rowling et al., "Arterial blood gas analysis: as safe as we think? a multicentre historical cohort study," ERJ open research, vol. 8, no. 1, 2022.
- [11] T. B. Tufan et al., "Performance analysis of a flexible hpts-based carbon dioxide sensor for transcutaneous blood gas monitoring," in 2023 IEEE Biomedical Circuits and Systems Conference (BioCAS), 2023, pp. 1–5.
- [12] J. Carrington et al., "Transcutaneous carbon dioxide monitoring could reduce physical contact with COVID-19 patients," American Journal of Hospital Medicine, Sep. 2021.
- [13] K. P. Sullivan et al., "Transcutaneous carbon dioxide pattern and trend over time in preterm infants," *Pediatric Research Nature Publishing Group*, pp. 1–7, Jan. 2021.
- [14] A. Jubran, "Pulse oximetry," Intensive care medicine, vol. 30, 2004.
- [15] I. Costanzo et al., "A prototype towards a transcutaneous oxygen sensing wearable," in 2019 IEEE Biomedical Circuits and Systems Conference (BioCAS). IEEE, 2019, pp. 1–4.

- [16] E. Zeserson et al., "Correlation of Venous Blood Gas and Pulse Oximetry With Arterial Blood Gas in the Undifferentiated Critically III Patient," *Journal of Intensive Care Medicine*, vol. 33, no. 3, pp. 176–181, 2018.
- [17] T. B. Tufan et al., "Implementation techniques for transcutaneous carbon dioxide monitoring: Approaches for wearable smart health applications," *IEEE Transactions on Biomedical Engineering*, 2023.
- [18] T. B. Tufan and U. Guler, "A Transcutaneous Carbon Dioxide Monitor Based on Time-Domain Dual Lifetime Referencing," *IEEE Transactions on Biomedical Circuits and Systems*, pp. 1–12, 2023.
- [19] I. Klimant et al., "Dual lifetime referencing (DLR)—a new scheme for converting fluorescence intensity into a frequency-domain or timedomain information," in New trends in fluorescence spectroscopy: applications to chemical and life sciences. Springer, 2001, pp. 257–274.
- [20] T. B. Tufan and U. Guler, "A Miniaturized Transcutaneous Carbon Dioxide Monitor Based on Dual Lifetime Referencing," in 2022 IEEE Biomedical Circuits and Systems Conference (BioCAS), Oct. 2022, pp. 144–148.
- [21] E. D. Chan et al., "Pulse oximetry: Understanding its basic principles facilitates appreciation of its limitations," *Respiratory Medicine*, vol. 107, no. 6, pp. 789–799, 2013.
- [22] B. Kahraman et al., "A miniaturized prototype for continuous noninvasive transcutaneous oxygen monitoring," in 2022 IEEE Biomedical Circuits and Systems Conference (BioCAS), 2022, pp. 486–490.
- [23] V. Vakhter et al., "A prototype wearable device for noninvasive monitoring of transcutaneous oxygen," *IEEE Transactions on Biomedical Circuits and Systems*, vol. 17, no. 2, pp. 323–335, 2023.
- Circuits and Systems, vol. 17, no. 2, pp. 323–335, 2023.
 [24] D. Dias and J. Paulo Silva Cunha, "Wearable health devices—vital sign monitoring, systems and technologies," Sensors, vol. 18, no. 8, p. 2414, 2018.
- [25] J. Jacquelin, "Régressions et équations intégrales," [Online]. https://www. researchgate. net/.../14674814-Regressions-et-equations-integrales. pdf, 2009.
- [26] B. Chieng et al., "A photoplethysmography wearable with long-term heart rate variability detection algorithm," in 2020 IEEE MIT Undergraduate Research Technology Conference (URTC). IEEE, 2020, pp. 1–4.
- [27] Analog Devices, "ADPD4100/ADPD4101 Multimodal Sensor Front End Datasheet Rev. 0," 2020.
- [28] Masimo, Rad-8 Signal Extraction Pulse Oximeter Operator's Manual MDSS GmbH, 2008, germany.
- [29] Sentec GmbH, Sentec Digital Monitoring System Instruction Manual, Sep. 2023, germany.
- [30] R. M. ApS, Radiometer TCM TOSCA/CombiM Operator's Manual, Nov. 2018, denmark.
- [31] G. Chuiko et al., "Oxygen saturation variability: Healthy adults," in 2019 XIth International Scientific and Practical Conference on Electronics and Information Technologies (ELIT). IEEE, 2019, pp. 72–75.